

THE INFLUENCE OF GRAZING FLOW ON THE RAYLEIGH CONDUCTIVITY OF AN APERTURE OF ARBITRARY SHAPE [†]

Sheryl M. Grace [†] and Michael S. Howe [‡] and Kelly P. Horan [¶]

Aerospace and Mechanical Engineering Department

Boston University

110 Cummington St., Boston, MA 02215

ABSTRACT

This research investigates the effect of geometry on the unsteady motion induced in a wall aperture by a pressure perturbation in the presence of grazing flow. For certain combinations of perturbation frequency, aperture size and flow speed, the aperture shear layer motion will augment the perturbation energy. Combining the three parameters into a Strouhal number, we see that for certain ranges of Strouhal number the coupling of the aperture dynamics and the mean flow leads to the production of sound and vibration. We examine this coupling for both one-sided and two-sided grazing flow past the aperture and consider several symmetric aperture geometries which include the circle, square, cross, triangle, rectangle, and one denoted as the crown. In this study we use the Rayleigh conductivity to analyze the Strouhal number dependence of the different aperture and flow configurations for a given time harmonic applied pressure disturbance. The model is valid in the low Mach number limit, and uses linearized theory. Using this model, we show that aperture geometry does not affect the Strouhal number range in which the aperture dynamics add energy to the flow perturbation. Similarly, the Strouhal number which approximately corresponds to self-oscillations of the shear layer remains relatively unchanged when the geometry of the aperture changes. Finally, we verify the reci-

procity relation in the sense that the orientation of the aperture in the streamwise direction does not affect the aperture shear layer behavior.

INTRODUCTION

Experimental research has shown that unsteady flow past wall apertures and cavities can create narrow band acoustic tones [1, 2]. Rossiter [1] was the first to attribute the tones to a feedback mechanism involving shed vorticity from the leading edge convecting across the aperture and interacting with the trailing edge to produce a pressure disturbance which travels back across the aperture. The tones which are produced correspond to continuous frequency ranges or Strouhal numbers in which the shear layer across the aperture exhibits unstable growth. A proper understanding of this phenomenon is important because of the wide range of mechanical systems in which this flow situation is present. Typical examples include, perforated baffles in cross-flow heat exchangers, depressions in submarine and ship hulls, computer boards with closely spaced chip carriers, aircraft control surfaces and fuselage openings, and flow-through resonators of automobile mufflers.

In this research we consider the low Mach number limit for the flow past a symmetric aperture of finite extent and study the response of the aperture shear layer to a disturbance such as incident sound or the pressure field of a large scale flow inhomogeneity. The mathematical model we use for this problem was developed in [2, 3]. It is an incompressible, inviscid, linearized, frequency-domain model in which the aperture shear layer is represented by a vortex sheet. Details of the model are provided in

[†]Copyright ©1997 by Sheryl Grace. Published by the American Institute of Aeronautics and Astronautics, Inc. with permission.

[‡]Assistant professor, Member AIAA.

[§]Professor, Member AIAA.

[¶]Research Assistant.

the second section of this paper.

The vortex sheet model was applied in [4] to investigate grazing flow over a slot of infinite span. For one-sided grazing flow, it was shown that energy of an applied, time-harmonic pressure force is dissipated by the production of vorticity in the slot except for Strouhal numbers $\epsilon = \frac{\omega L}{U^+}$ between 1.59 and 3.49 (L is one half of the distance from the most upstream point of the aperture to the most downstream point, and U^+ is the speed of the flow). In this interval energy is extracted from the mean flow and supplied to the imposed pressure field. This frequency range is centered approximately on the minimum frequency of self-sustained oscillations of the shear layer in the slot. When the mean velocities are the same on both sides of the slot, energy is extracted from the mean flow whenever the Strouhal number lies within one of the intervals $2.4 + n\pi < \frac{\omega L}{U^+} < 3.7 + n\pi$, where n is an integer greater than 0 (here U^+ is the larger of the two flow velocities).

Scott extended this work on the slot by considering a circular aperture in the presence of grazing flow [2, 3]. It was shown that one sided flow over a circular aperture is unstable for Strouhal numbers between 2.0 and 3.6. When the flow is the same on both sides, the behavior becomes periodic in frequency when the Strouhal number exceeds about 3.5, and perturbation energy is alternately augmented and attenuated by the coupling with the mean flow.

An approximate treatment of *tapered* apertures was discussed in [5], with particular attention to trapezoidal apertures, the extreme limiting cases being apertures of rectangular and triangular cross-sections. Using the averaging method the results showed that as the taper was increased the range of Strouhal numbers for which the aperture was supplying energy to the perturbation also increased. It was also stated, that due to reciprocity, the trapezoid could be oriented either with its longer side as the leading edge or with the shorter side as the leading edge and both aperture configurations would behave the same.

In this research we show that aperture shape does *not* significantly alter the range of Strouhal frequencies for which the shear layer provides energy to the flow perturbation. We also show that the Strouhal number which corresponds to self-oscillation is not significantly changed by aperture geometry. Finally, we validate the reciprocity relation discussed in [5].

FORMULATION

Nominally steady flow past an aperture with dif-

ferent flow speeds over each face is unstable. For an aperture of infinite extent, the growth of an arbitrarily small perturbation tends to be dominated by the appearance of interfacial *Kelvin-Helmholtz* waves whose wavenumbers correspond to the most unstable waves of the mean shear layer [7]. When the aperture area is finite, however, the shear layer instability depends critically on feedback which occurs between the aperture's leading and trailing edges. This feedback loop consists of the shedding of vorticity from the leading edge, the convection of the vorticity across the aperture, the production of a pressure pulse when the vorticity interacts with the trailing edge of the aperture and the traversing of that pressure pulse back across the aperture to the leading edge. This feedback will either reinforce or inhibit vortex shedding depending on the phasing of the feedback signal relative to that of natural shedding from the leading edge. This view of the motion is precisely that advanced many years ago by Rossiter [1] from his experimental investigation of tones and buffeting occurring during high speed flow over a wall cavity. As a corollary, one might conclude that when the flows over both faces of the aperture are equal (so that there is no mean shear in the aperture mouth), the motion becomes stable. In practice, however, finite wall thickness and the turbulent wall boundary layers will produce unsteady shedding of vorticity from the aperture leading edge. Hence, an instability may arise, but it will be much weaker than when the flows over both faces differ.

In order to completely quantify this qualitative picture of disturbed motion of the shear layer it is necessary to solve the fully viscous, nonlinear equations of fluid motion. This is the case, for example, if one wants to determine the amplitude of a possible self-sustaining, quasi-periodic mode of the aperture motion. If, however, it is required only to calculate the *frequencies* of these oscillations (which correspond to the frequencies that dominate the production of sound and vibration by the flow), it is sufficient in a first approximation to consider a linearized representation of the shear layer motion. This result stems from the domination of the feedback cycle by the convection velocity of vorticity across the mouth of the aperture, which is found experimentally to be essentially independent of the amplitude of the motion [8, 9, 10, 11]

The present study is restricted to low Mach number flows, for which it is permissible to regard the unsteady motion in the aperture as incompressible. Furthermore, comparisons between experimental results and simple approximate schemes [2, 5] indicate

that the motion may be regarded as inviscid except insofar as its influence is incorporated by means of the standard application of the Kutta condition at the leading edge of the aperture.

The stability properties of the aperture shear layer can be examined in this inviscid approximation by considering the linearized motion induced by an externally applied, time harmonic pressure force. This force initiates the production of unsteady vorticity at the aperture leading edge. In the inviscid approximation a vortex sheet spans the aperture in the undisturbed state, and additional vorticity is shed under the influence of the applied pressure. The stability of the motion can be analyzed by considering the equation governing the displacement of the vortex sheet from its planar form, for which the instability frequencies coincide with the eigenvalues of this equation.

The linear stability characteristics of the shear flow over an aperture govern the properties of the *Rayleigh conductivity*, denoted as $K_R(\omega)$, which is the reciprocal of the aperture impedance [12]. For time harmonic pressures $p_o^+ e^{-i\omega t}$ and $p_o^- e^{-i\omega t}$ applied above and below the aperture respectively, the Rayleigh conductivity is defined by the relation

$$K_R(\omega) = \frac{i\omega\rho_0 Q(\omega)}{p_o^+(\omega) - p_o^-(\omega)} \quad (1)$$

where Q is the volume flux at the aperture, $p_o^+ - p_o^-$ is the applied pressure difference across the aperture, ω is the radian frequency, and ρ_0 is the fluid density [12].

The pressure difference produces a small amplitude displacement ζ of the vortex sheet from its undisturbed form. Thus, in the linearized approximation and in terms of the coordinate system shown in Figure 1, the aperture volume flux is given by

$$\begin{aligned} Q &= \int_{-\infty}^{\infty} \int_{-\infty}^{\infty} -i(\omega + iU^+ \frac{\partial}{\partial y_1}) \zeta(y_1, y_2, 0) dy_1 dy_2 \\ &= \int_{-\infty}^{\infty} \int_{-\infty}^{\infty} -i(\omega + iU^- \frac{\partial}{\partial y_1}) \zeta(y_1, y_2, 0) dy_1 dy_2 \\ &\equiv -i\omega \int_{-\infty}^{\infty} \int_{-\infty}^{\infty} \zeta(y_1, y_2, 0) dy_1 dy_2 \end{aligned} \quad (2)$$

since ζ vanishes on the wall.

The eigenvalues of the equation governing the aperture shear layer displacement are identical to the poles of the Rayleigh conductivity function. Hence,

the real parts of the poles of $K_R(\omega)$ in the complex frequency plane coincide with the linear instability frequencies of the aperture motion [13], and determine the Strouhal numbers of a possible self-sustaining oscillation and the frequencies of the narrow band tones radiated into the flow. In the absence of mean flow K_R is a real valued quantity that depends only on the shape and size of the aperture.

To calculate the conductivity according to (1) we must first calculate the displacement ζ of the vortex sheet. To do this we make use of the procedure used by Scott [2, 3] for a circular aperture. The incompressible motion on either side of the sheet depends on the solution of the Laplace equation

$$\nabla^2 \Phi^\pm = 0 \quad (3)$$

for the velocity potential Φ . The unsteady pressure induced by the motion of the vortex sheet is then obtained from the linearized Euler equation in the form

$$p^+ = +i\rho_0(\omega + iU^+ \frac{\partial}{\partial x_1})\Phi^+, \quad x_3 > 0 \quad (4)$$

$$p^- = +i\rho_0(\omega + iU^- \frac{\partial}{\partial x_1})\Phi^-, \quad x_3 < 0. \quad (5)$$

The condition that the pressure is continuous across the vortex sheet accordingly implies that

$$\begin{aligned} p_o^+ + i\rho_0(\omega + iU^+ \frac{\partial}{\partial x_1})\Phi^+ \\ = p_o^- + i\rho_0(\omega + iU^- \frac{\partial}{\partial x_1})\Phi^-, \quad x_3 = 0 \end{aligned} \quad (6)$$

The solution of Laplace's equation (3) is obtained by application of Green's Theorem using a Green's function whose normal derivatives vanish on $x_3 = 0$ and $y_3 = 0$, i.e.,

$$\Phi^\pm(\vec{x}) = \mp \int_{-\infty}^{\infty} \frac{\partial \Phi^\pm}{\partial y_3} G(\vec{x}|\vec{y}') dy_1 dy_2, \quad \vec{y}' = (y_1, y_2, 0) \quad (7)$$

$$\begin{aligned} G(\vec{x}|\vec{y}') &= -\frac{1}{4\pi} \left[\frac{1}{|\vec{x} - \vec{y}'|} + \frac{1}{|\vec{x} - \vec{y}''|} \right], \\ \vec{y}'' &= (y_1, y_2, -y_3). \end{aligned}$$

By substituting the relation

$$\frac{\partial \Phi^\pm}{\partial y_3} = -i(\omega + U^\pm \frac{\partial}{\partial x_1})\zeta$$

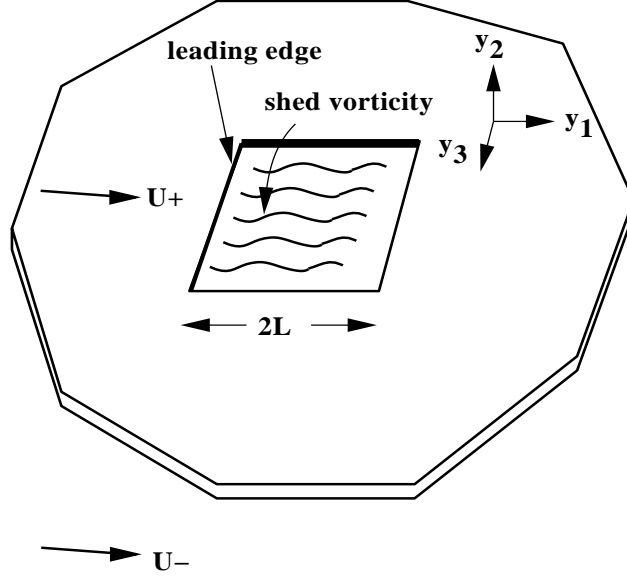


Figure 1: Grazing flow past a wall aperture.

into (7), and integrating by parts, we find that equation (6) can be cast in the form

$$\frac{p_o^+ - p_o^-}{\rho_0} = \frac{1}{2\pi} \left[(\omega + iU^- \frac{\partial}{\partial x_1})^2 + (\omega + iU^+ \frac{\partial}{\partial x_1})^2 \right] \times \int_s \frac{\zeta(y_1, y_2, 0)}{|\vec{x} - \vec{y}|} dy_1 dy_3 \quad (8)$$

where the integration is restricted to the aperture opening. To simplify this, we introduce the following nondimensionalization and rescaling where lengths are nondimensionalized by the half length of the aperture in the streamwise direction and velocities by U^+ which is the larger flow velocity:

$$\vec{X}, \vec{Y}, Z = \vec{x}/L, \vec{y}/L, \zeta/L \quad (9)$$

$$\epsilon = \omega L / U^+ \quad (10)$$

$$U_r = U^- / U^+ \quad (11)$$

$$Z' = \frac{Z \rho_0 \epsilon^2 U^{+2}}{\pi(p_o^+ - p_o^-)} \quad (12)$$

where ϵ is the Strouhal number. Then, by integrating (8) with respect to the second order differential operator on the right hand side, we obtain

$$\int_s \frac{Z'(Y_1, Y_2, 0)}{|\vec{X} - \vec{Y}|} dY_1 dY_2$$

$$= 1 + \alpha(X_2)e^{i\epsilon_1 X_1} + \beta(X_2)e^{i\epsilon_2 X_1} \quad (13)$$

Here α and β are unknown functions of X_2 which must be determined to ensure that the Kutta condition is satisfied at the leading edge of the aperture [2, 3]; ϵ_1 and ϵ_2 are the nondimensional Kelvin-Helmholtz wave numbers for a velocity discontinuity [7],

$$\epsilon_1 = \frac{\omega L(1+i)}{U^+ + iU^-}, \quad \epsilon_2 = \frac{\omega L(1-i)}{U^+ - iU^-}. \quad (14)$$

Note that $\epsilon_1 = \epsilon_2 = \epsilon$ when $U^+ = U^-$. In this case the right hand side of Equation (13) can be reduced to

$$1 + \alpha(X_2)e^{i\epsilon X_1} + \beta(X_2)X_1 e^{i\epsilon X_1}$$

The integral equation (13) is solved by means of a standard quadrature scheme which is discussed in the next section.

NUMERICAL IMPLEMENTATION

In this research we solve the two-dimensional governing integral equation (13) numerically in order to obtain the Rayleigh conductivity for various symmetric aperture shapes. The equation is discretized by covering the aperture with a cartesian grid as shown by the schematic in Figure 2. On each grid cell $Z'(Y_1, Y_2, 0)$ is assumed to be constant, but Green's function is integrated analytically. The Kutta condition is imposed by requiring that $\zeta = 0$ (which is the

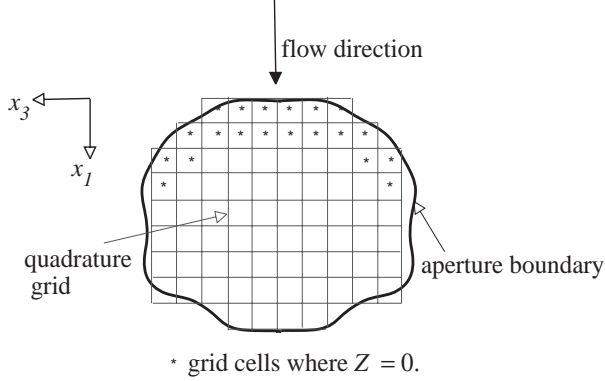


Figure 2: Grid used in quadrature of integral equation with the locations for the application of the Kutta condition marked.

same as imposing $Z' = 0$) on the first two grid cells in each grid row of constant Y_2 ; this is equivalent to requiring that the displacement of the vortex sheet and its streamwise derivative vanish at the leading edge. The first two Z' values in each grid row may then be replaced by the unknown functions $\alpha(Y_2)$ and $\beta(Y_2)$ which are constant for each grid row (of constant Y_2).

When Z' , α and β have been determined using a complex matrix solver, the scaled conductivity, \tilde{K}_R , is calculated using the following simple integration technique

$$\begin{aligned} \tilde{K}_R(\omega) &= \frac{K_R(\omega)\rho_0\epsilon^2U^{+2}}{\pi(p_o^+ - p_o^-)} = \pi L \int \int_S Z' dS \\ &= \pi L \sum_{i=1}^{\infty} \sum_{j=1}^{\infty} Z'(Y_{1i}, Y_{2j}) dY_1 dY_2 \end{aligned} \quad (15)$$

RESULTS

We have considered numerous symmetric aperture shapes, and have calculated the scaled Rayleigh conductivity ($\tilde{K}_R = 2L(\zeta - i\Delta)$) for both one-sided and two-sided equal grazing flow with time harmonic applied pressures $p_o^+ = P_I e^{-i\omega t}$, $p_o^- = 0$. The shapes we consider include the circle, square, cross, two sizes of forward triangles (upstream pointing) and backward triangles (downstream pointing), crown, and rectangle as shown in Figure 3.

The cross-sectional geometries we have studied were chosen for several reasons. We use the circle and tapered apertures as a benchmarking tool for our numerical code. The cross-shaped aperture was suggested by Chanaud [14]. The crown was tested in hopes that it would modify the vortex shedding

from the leading edge of the aperture and cause a significant shift in the self-oscillation frequency.

For flow past just one face of the aperture, the components of the scaled conductivity, ζ and Δ , are plotted vs. the Strouhal number, in Figures 4 and 5. As was noted earlier, it is the real part of the poles of the conductivity function which correspond to the self-oscillation frequencies. These approximately coincide with the minima in Δ . And the regions where $\Delta < 0$ indicate regions where the aperture shear layer supplies energy to the applied pressure perturbation. Hence, these are the regions of instability for the aperture shear layer. As the Strouhal number increases the magnitude of the square root singularity in ζ near the trailing edge of the aperture increases (for the case of one-sided flow past the aperture). This makes the numerical evaluation of ζ and the subsequent integration inaccurate past a Strouhal number of about 5. Therefore we only show values for the conductivity corresponding to Strouhal numbers of 0 to 5.

For the one-sided flow case, there is one continuous region of Strouhal numbers in which $\Delta < 0$; and, the location of the minimum in this region varies only slightly for the different aperture geometries. We also observe that the jagged leading edge of the crown aperture does not affect the shed vorticity enough to greatly change the dependence of the shear layer motion on Strouhal number. Finally, we observe that the conductivity is independent of the orientation of the triangular-shaped apertures (upstream pointing or downstream pointing). This supports the reciprocity relation discussed in [5].

All of these points are made more clearly when the data is plotted simultaneously. To make a fair comparison on one single plot, it is necessary to normalize the scaled conductivity by the square root of the aperture area rather than 2 times the half length in the streamwise direction. Figure 6 shows the comparison of \tilde{K}_R/\sqrt{A} vs. Strouhal number for the circle, square, cross, crown and rectangle. Figure 7 shows the comparison for the large and small forward and backward facing triangles. Some numerical error is present for the small forward triangle at the higher Strouhal numbers. This is a result of the difficulty in capturing the leading edge Kutta condition using a rectangular grid to discretize an aperture with such a sharp point. By refining the grid, this error is minimized.

We then considered equal flow on both faces of the apertures. For the two-sided grazing flow, the problem is numerically stable and we can calculate ζ and its integral for very high Strouhal numbers.

We choose here to use Strouhal numbers from 0 to 15. Figures 8 and 9 show σ and Δ for all of the aperture shapes. Again the similarity between the results is clear. The minima of Δ all occur at roughly the same values of ϵ , as shown more clearly in the renormalized simultaneous graphs in Figures 10 and 11. One difference however, is that for the case of the large triangular apertures, Δ first becomes negative at about $\epsilon = 10.3$ as compared to $\epsilon = 2.5$ for the other geometries. More research is needed to fully understand this behavior. Comparing the results for the forward and backward triangles as shown in Figure 11 again we see that reciprocity is affirmed.

A final interesting point can be made for the equal two-sided flow case. The overall trends in the conductivity directly reflect the general elements of the geometry of the aperture. For some of the apertures, the magnitude of the maxima and minima in the real and imaginary parts of the conductivity remain the same value indefinitely, e.g. square, and rectangle. However, for those apertures, whose length from leading edge to trailing edge continuously decreases with span, the values of the maxima and minima decrease with ϵ , e.g. circle, and triangles. For the cross-shaped aperture, where there are two distinct lengths in the streamwise direction, there are two distinct values of the peaks in the conductivity which continue repeating indefinitely. The crown-shaped aperture is a mix of all of these. There are two main lengths which are reflected in the conductivity, but since there is a gradual change between the two lengths, the values of the corresponding maxima and minima decrease with epsilon.

In a frequency domain calculation we cannot calculate the magnitude of the instabilities, only the associated frequencies, but it is surmised that these varying values in the maxima and minima may give a qualitative description of the magnitude of the instabilities. The validity of this statement is left for future investigations.

CONCLUSIONS

Grazing flow past a wall aperture with the addition of a time harmonic applied pressure perturbation creates unsteady motion in the aperture shear layer. The shear layer behavior can both augment and attenuate the energy in the flow perturbation depending upon the coupling between the motion and the mean flow. Of particular interest are the Strouhal number ranges which correspond to augmentation of the perturbation energy since it is these frequencies which dominate the production of sound and vibration. Here the Strouhal number is based

on the frequency of the applied pressure disturbance, the half length of the aperture in the streamwise direction and the velocity of the flow past the aperture.

The aperture dynamics are reflected in the Rayleigh conductivity insofar as the real parts of the complex poles of this function correspond to the self-oscillating frequencies. Studying the Rayleigh conductivity for solely real frequencies, still allows us to predict the various Strouhal regions and to estimate the self-oscillating frequencies. This is done by studying the imaginary part of the Rayleigh conductivity. When it is less than zero, the aperture shear layer motion serves to enhance the applied pressure disturbance. The minima of these regions occur approximately at the Strouhal numbers which correspond to self-oscillation.

We study finite apertures of various shapes and consider the cases when there is flow past only one face of the aperture and when there is equal flow on both faces of the aperture. The shapes discussed in this report include the circle, square, cross, large and small forward triangles, large and small backward triangles, crown and rectangle. We show that the range of Strouhal numbers associated with the perturbation energy enhancement and in particular the Strouhal number that is associated with self-oscillation of the aperture shear layer remain relatively unchanged as the shape of the aperture changes (for both the one-sided and two-sided flow cases). Furthermore using the forward and backward facing triangles we verify the reciprocity relation that states that the streamwise orientation of the aperture is immaterial. We also show that a qualitative assessment of the geometry of the aperture can be made from the general trends in the Rayleigh conductivity for the two-sided flow case. The distinct number of values taken by the minima or maxima indicates the number of length scales present in the aperture geometry in the streamwise direction. For example, the Rayleigh conductivity for the cross-shaped aperture shows two distinct minima values.

ACKNOWLEDGMENTS

The authors would like to thank Kadin Tseng, consultant at the Boston University Scientific Computing and Visualization facility, for his assistance with the numerical implementation.

REFERENCES

- [1] J. E. Rossiter, (1964), "Wind tunnel experiments of the flow over rectangular cavities at subsonic and transonic speeds," *Aero. Res.*

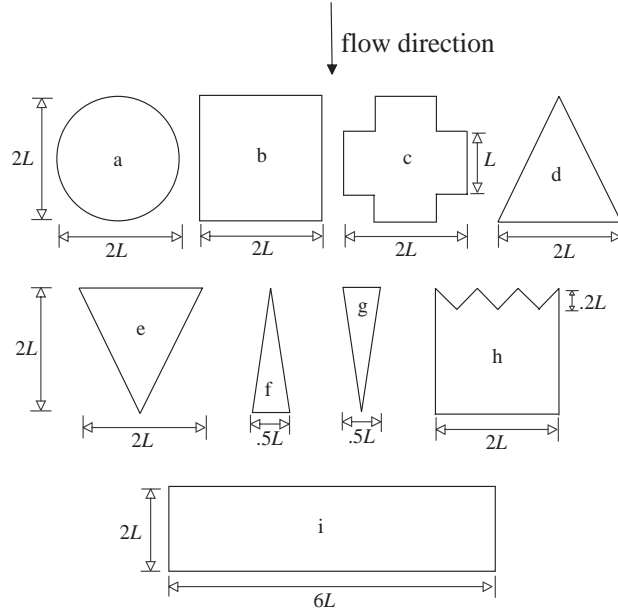


Figure 3: Aperture cross-sections studied. a) circle, b) square, c) cross, d) forward pointing triangle, e) backward pointing triangle, f) smaller forward pointing triangle, g) smaller backward pointing triangle, h) crown, i) rectangle with aspect ratio 3.

- Counc. R&M*, no. 3438.
- [2] M. S. Howe, M. I. Scott and S. R. Sipcic, (1996), "The Influence of Tangential Mean Flow on the Rayleigh Conductivity of an Aperture," in *Proceedings of the Royal Society of London A* 452, 2303 - 2317.
- [3] M. I. Scott, (1995), "The Rayleigh Conductivity of A Circular Aperture in The Presence of A Grazing Flow," *Master's Thesis*, Boston University.
- [4] M. S. Howe, (1981), "On the Theory of Unsteady Shearing Flow Over a Slot," *Philosophical Transactions of the Royal Society of London*, Vol. A-303.
- [5] M. S. Howe, (1996), "Influence of Cross-Sectional Shape on the Conductivity of a Wall Aperture in Mean Flow," *Boston University Technical Report*, No. AM-96-034, Nov.
- [6] M. S. Howe, (1996), "Influence of Wall Thickness on Rayleigh Conductivity and Flow-Induced Aperture Tones," *Boston University Technical Report*, No. AM-96-022, Sept. *J. Fluids and Structures* (in press)
- [7] Sir H. Lamb, (1995), *Hydrodynamics, 6th Ed.*, Cambridge University Press, New York, pg. 373.
- [8] A. Powell, (1961), "On the edgetone," *Journal of the Acoustical Society of America*, Vol. 33, pp. 395 - 409.
- [9] D. K. Holger, T. A. Wilson, and G. S. Beavers, (1977), "Fluid mechanics of the edgetone," *Journal of the Acoustical Society of America*, Vol 62, pp. 1116 - 1128.
- [10] D. Rockwell, (1983), "Oscillations of Impinging Shear Layers," *AIAA Journal*, Vol. 21, pp. 645 - 664.
- [11] W. K. Blake, and A. Powell, (1986), "The Development of Contemporary Views of Flow-tone Generation", pp. 247 - 325 of *Recent Advances in Aeroacoustics*, (edited by A. Krothapali and C. A. Smith). Springer.
- [12] J. W. S. Rayleigh, (1945), *The Theory of Sound*, Vol. 2, Dover, pg. 173.
- [13] M. S. Howe, (1996), "Edge, cavity and aperture tones at very low Mach numbers," *Journal of Fluid Mechanics* Vol. 330, 61 - 84.
- [14] R. C. Chanaud, (1994), "Effects of geometry on the resonance frequency of Helmholtz resonators," *Journal of Sound and Vibration*, Vol. 178. no. 3, pp. 337-348.

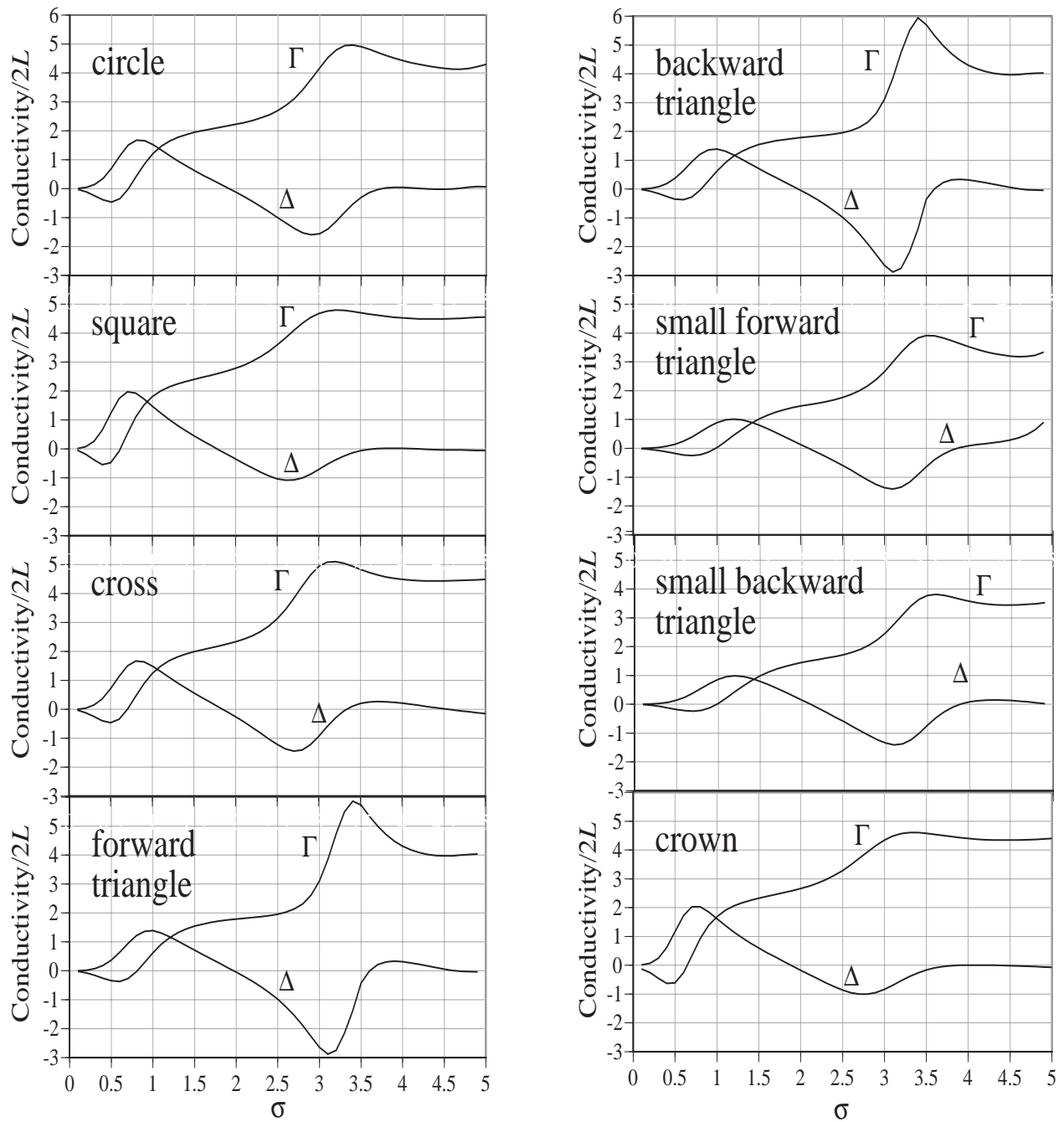


Figure 4: The Rayleigh conductivity for one-sided grazing flow past aperture with shapes circle, square, cross, forward triangle, backward triangle, small forward triangle, small backward triangle, and crown.

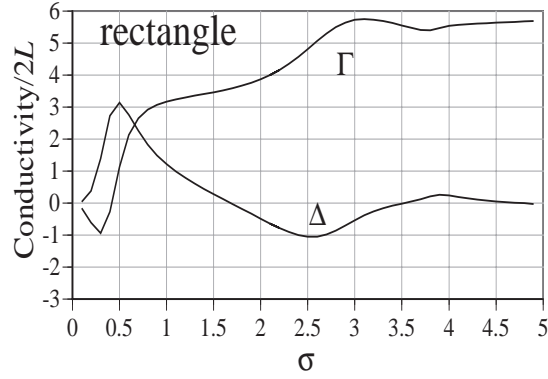


Figure 5: The Rayleigh conductivity for one-sided grazing flow past the rectangular aperture.

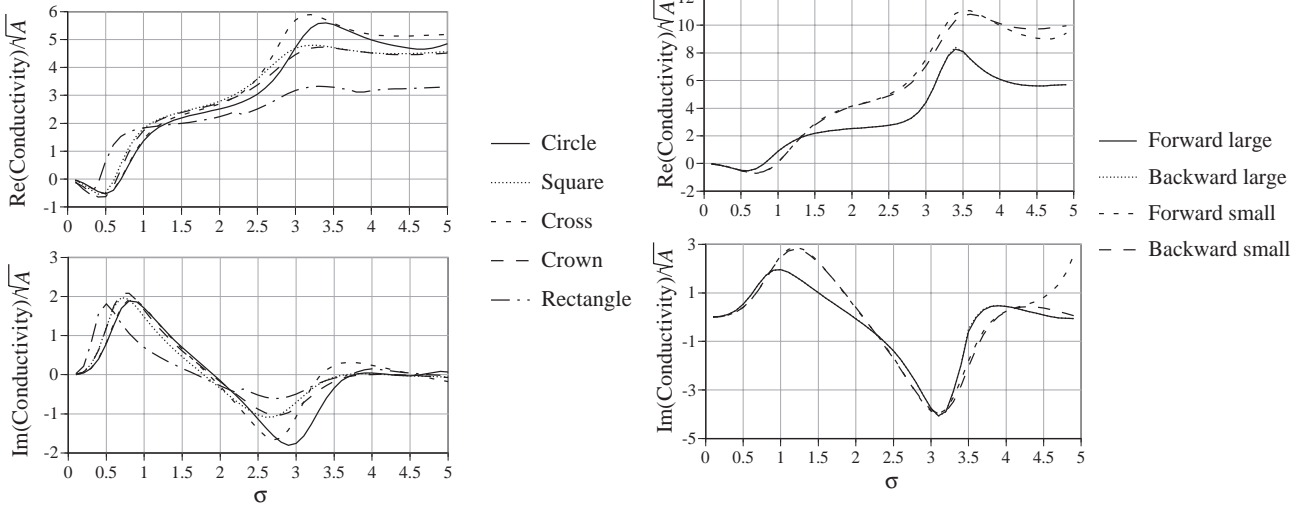


Figure 6: Real part (top) and imaginary part (bottom) of the Rayleigh conductivity normalized by the square root of the area for circle, square, cross, crown and rectangle apertures with flow on one side.

Figure 7: Real part (top) and imaginary part (bottom) of the Rayleigh conductivity normalized by the square root of the area for the large and small, forward and backward facing triangle apertures with flow on one side.

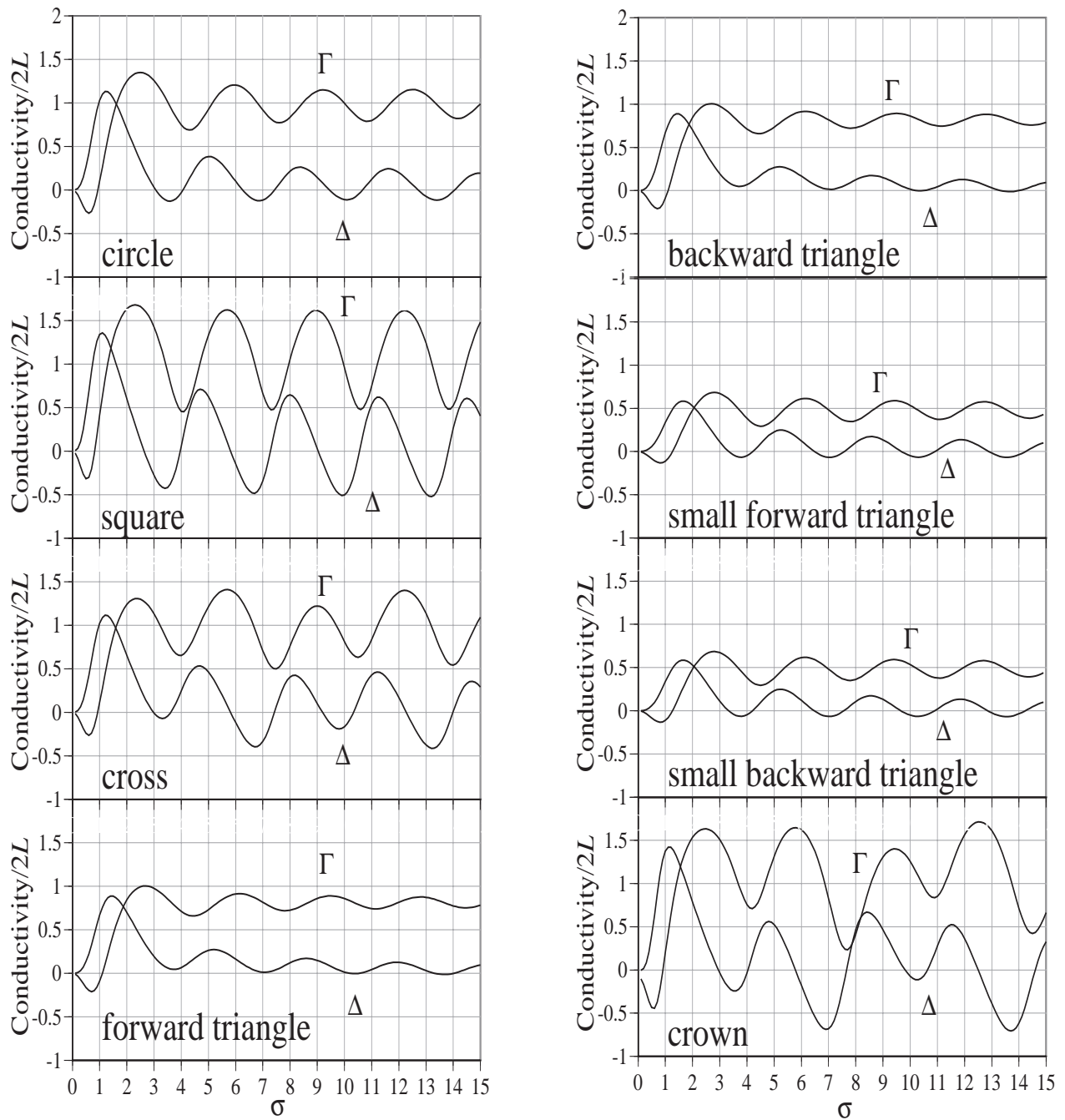


Figure 8: The Rayleigh conductivity for equal two-sided grazing flow past apertures with shapes: circle, square, cross, forward triangle, backward triangle, small forward triangle, small backward triangle and crown.

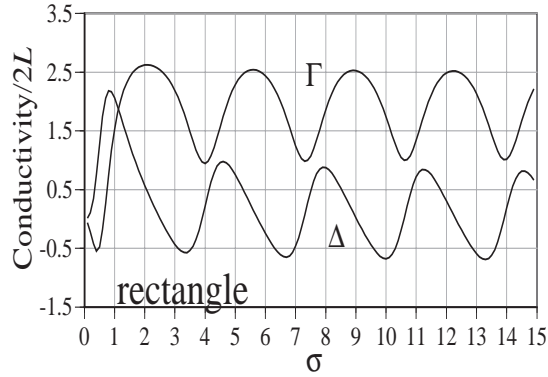


Figure 9: The Rayleigh conductivity for equal two-sided grazing flow past the rectangular aperture.

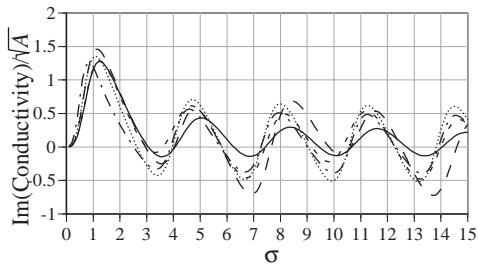
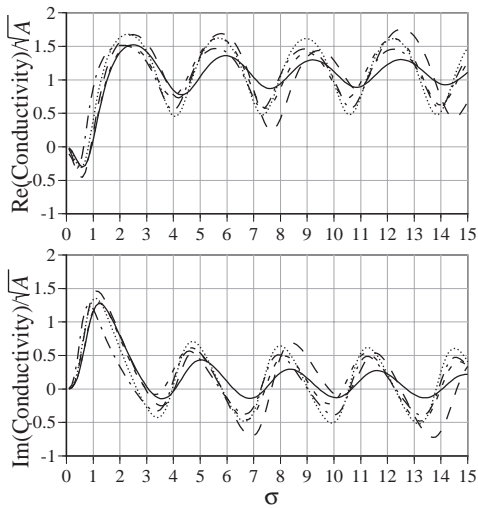


Figure 10: Real part (top) and imaginary part (bottom) of the Rayleigh conductivity normalized by the square root of the area for circle, square, cross, crown and rectangle apertures with equal flow on both faces.

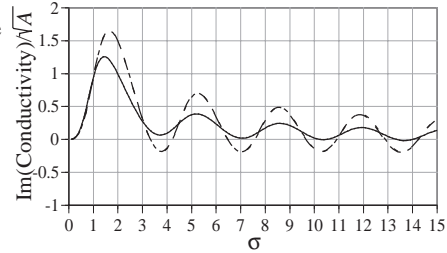
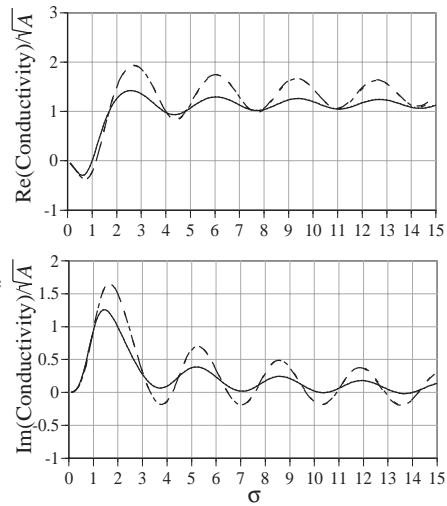


Figure 11: Real part (top) and imaginary part (bottom) of the Rayleigh conductivity normalized by the square root of the area for the large and small, forward and backward facing triangle apertures with equal flow on both faces.